Temporal variability in transmission spectra of H2-dominated exoplanets: the influence of thermal evolution and stellar irradiation on atmospheric composition

Kecskeméthy, V.; Louca, A.J.; Miguel, Y.

New Astronomy 113 (2024) 102296

Contents lists available at ScienceDirect

New Astronomy

journal homepage: www.elsevier.com/locate/newast

Temporal variability in transmission spectra of H_2-dominated exoplanets: The influence of thermal evolution and stellar irradiation on atmospheric composition

Viktória Kecskeméthy [a], Amy Louca [a], Yamila Miguel [b,a,*]

[a] Leiden Observatory, Leiden University, PO Box 9513, 2300 RA Leiden, The Netherlands
[b] SRON Netherlands Institute for Space Research, Niels Bohrweg 4, 2333 CA Leiden, The Netherlands

ARTICLE INFO

Keywords:
Planets and satellites
Atmospheres
Composition
Gaseous planet
Planet-star interactions

ABSTRACT

Planets and their host stars undergo evolutionary changes over time, resulting in variations in internal temperature and incoming radiation, which significantly impact the temperature structure and composition of their atmospheres. These evolving conditions give rise to distinctive features in planetary spectra that are observable only during specific stages of planetary evolution. We aim to understand how the composition of planets with H_2-dominated atmospheres changes over longer timescales due to their thermal evolution. We also investigate time-dependent features in the transmission spectra. These features could provide insights in both the formation and evolution of these gaseous planets, as well as the timescales of these changes, enabling us to study the potential variability of exoplanets over time. We evolve a ~0.04 M_{Jup} and ~0.45 M_{Jup} planet around a 1.0 $M_{\odot}$ and 1.3 $M_{\odot}$ star respectively for $10^{9.5}$ years. In both systems, the planets are considered at semi-major axes of 0.1 AU and 1.0 AU. The star-planet systems are evolved by making use of Modules for Experiments in Stellar Astrophysics (MESA). The temperature–pressure profiles are obtained at selected time-steps using an analytical approximation based on the internal and irradiation temperature of the planet at each time step. We then use VULCAN, a photochemical kinetics code, to see how the composition changes with time in the atmosphere due to the thermal evolution of the planets. By making use of the radiative transfer code petitRADTrans, we also simulate the evolution of the transmission spectra of the planets to find potential time-dependent spectral features. Our findings show a prominent change in the CO_2 feature at ~ 4.3μm. For the 0.45 M_{Jup} case, this feature is visible in the pre-main-sequence phase of the host star, regardless of orbital distance from the host star. In the case of the ~0.04 M_{Jup} planet, this CO_2 feature is visible until $t \leq 10^6$ years, and then it reappears after $t \geq 10^8$ years when the planet is 0.1 AU away the host star. The CH_4 features at ~ 3.3μm and ~ 7.5μm are only time-dependent when the planet is located at 0.1 AU from the host star and experiences high irradiation since the high temperature at early stages favoured CO_2 over CH_4. When the planet is 1.0 AU away from its host star, the CH_4 features are always visible regardless of the mass and hence internal temperature of the planet.

1. Introduction

In the era of space telescopes, such as the James Webb Space Telescope (JWST), and ground-based telescopes, we find ourselves in an unprecedented age of discovery. Recent studies have shown the potentials of JWST which opened up new avenues for exoplanets in both the theoretical as well as the observational point of view (e.g., Fauchez et al., 2022; Birkmann et al., 2022; Feinstein et al., 2023; Alderson et al., 2023; Rustamkulov et al., 2023; Ahrer et al., 2023; Carter et al., 2023). The spectral characterisation of exoplanets is key to better understanding their formation and evolution. It remains challenging to attribute the currently observed spectral features to solely formation models or evolution models. The research presented here is focused on better understanding the planetary processes behind the observed spectral features by centralising the impact of evolution models on observed spectra.

Analytical (e.g. Guillot, 2010) and radiative transfer (e.g. Baraffe et al., 2003; Fortney et al., 2011) evolution models of gaseous planets, that took both the irradiated atmospheric structure and interior structure into account, showed the importance of irradiation as it significantly changes the properties of the planet. They showed that

* Corresponding author.
E-mail address: ymiguel@strw.leidenuniv.nl (Y. Miguel).

https://doi.org/10.1016/j.newast.2024.102296
Received 23 January 2024; Received in revised form 4 August 2024; Accepted 13 August 2024
Available online 21 August 2024

Table 1
The star-planet systems. The columns are: the labelling of the system as they are shown in the figures, mass of the planet, distance from the host star, mass of the host star.

	M_p (M_{Jup})	a (AU)	M_s ($M_\odot$)
Case A1:	0.45	0.1	1.3
Case A2:	0.45	1.0	1.3
Case B1:	0.04	0.1	1.0
Case B2:	0.04	1.0	1.0

the main effect of irradiation is the increased temperature in the outer layers of the planetary atmosphere, decreasing the temperature gradient between the upper and lower atmospheric levels.

The chemistry of planetary atmospheres and their spectral features are deeply affected by both the temperature structure within the atmosphere and the stellar luminosity that affects photochemical processes (e.g., Madhusudhan, 2019; Zahnle et al., 2009; Moses et al., 2011; Venot et al., 2012; Rimmer and Helling, 2016; Drummond et al., 2016; Hobbs et al., 2019; Shulyak et al., 2020; Tsai et al., 2023) among other factors.

In this study, we focus on the impact of thermal planetary evolution on the chemical composition of exoplanet atmospheres and the implications on their transmission spectra. We explore how the composition and spectral features of four different hydrogen-dominated planets change over ~3.1 Gyr by varying their semimajor axes and/or host star sizes. This is done by simulating their thermal profiles due to the planet's evolution and factoring in the stellar evolution process. Through our research, we identify and analyse time-dependent spectral features, providing insights into the evolution of H_2-dominated gaseous planets. We place special emphasis on the CO_2 feature at 4.3 μm, because CO_2 is an important tracer of planet formation as it helps us to determine the solid versus gaseous material ratio during its formation (Lodders and Fegley, 2002; JWST Transiting Exoplanet Community Early Release Science Team et al., 2023).

The structure of the paper is the following: Section 2 describes the star-planet systems that are taken into account, and how their evolution is modelled. In Section 3 we present the evolution of the atmospheric composition of the planets and their observability. In Section 4 we discuss the limitations of this study. A conclusion of this paper can be found in Section 5.

2. Methods

2.1. Planetary systems

We evolve gaseous planets of varied masses for $10^{9.5}$ yr at various distances from their host star. We consider two different planets with a mass of a $M_p = 0.04\ M_{Jup}$ and $M_p = 0.45\ M_{Jup}$, to see the effects of different internal temperature on planets with different masses. The lower mass planet orbits a solar-like star with a mass of $M_s = 1.0\ M_\odot$, and the higher mass planet orbits a larger and hotter star of spectral F-type, with $M_s = 1.3\ M_\odot$. In each planet-star system, we model our hypothetical planet with two different distances. The semimajor axes, a, between the planets and their host stars are 0.1, and 1.0 AU. By simulating the planets with the mentioned orbital distances around G-, and F-type host stars, the effect of high irradiation can be explored. All planets are H_2-dominated and assumed to have solar abundances taken from Lodders et al. (2009). A summarised overview of the cases can be found in Table 1. We note that in this study we do not take into account any possible migration that the planets might experience during the first years of their evolution.

2.2. Thermal evolution

We focus on how the atmospheric chemistry and observable features on the transmission spectra change by evolving the planetary temperature and pressure profile using the analytical approximation by Heng et al. (2014). Here they took into account the incoming radiation from the host star and the thermal emission of the planetary atmosphere and included non-isotropic scattering in their calculations. The longwave opacity (κ_L), shortwave opacity (κ_S), shortwave scattering parameter (β_S), and longwave scattering parameter (β_L) are set to 0.1, 0.02, 1.0, 1.0, respectively, and we only change the internal and irradiation temperature at various timesteps. The timesteps range from $10^{4.5}$ to $10^{9.5}$ yr in increments of 0.5 on the exponent. The values for the internal temperature are obtained by making use of the open source stellar evolution code, Modules for Experiments in Stellar Astrophysics (MESA), which is widely used for the evolutionary study of both stars (Paxton et al., 2010) and planets (Paxton et al., 2013). The stars are evolving with solar metallicities for $10^{9.5}$ yr, which is approximately the end of their main-sequence phase. We assume that the planets are made of a core of 10 $M_\oplus$ surrounded by a homogeneous envelope.

Assuming zero albedo, the irradiation temperature T_{irr} can be calculated using

$$T_{irr} = \sqrt{\frac{R_s}{2a}}T_{eff}, \quad (1)$$

where both the effective temperature of the host star (T_{eff}) and stellar radius (R_s) are obtained from MESA at each time step.

2.3. Chemical model

To model the mixing ratios of the atmosphere, the open-source photochemical kinetics code VULCAN[1] is used (Tsai et al., 2017, 2021). For case A1, the default validated N–C–H–O photo-chemical network is used, which includes 948 reactions containing 74 species. For the other cases we also include condensation as those are colder systems. Furthermore, we make use of the default solar spectrum from Gueymard (2018) for the one solar mass star. For the 1.3 solar mass star, the synthetic spectra is taken from PHOENIX (Husser et al., 2013), assuming an effective temperature of 6400 K. The spectra are scaled according to the orbital distance of the planet from the host star. We assume a constant eddy diffusion (K_{zz}) of 1e10 $cm^2\ s^{-1}$ (Moses et al., 2011; Parmentier et al., 2013; Miguel and Kaltenegger, 2014). For initial abundances we assume chemical equilibrium, and calculate it using the open source chemical equilibrium code, FastChem[2] (Stock et al., 2018).

2.4. Transmission spectra

The spectral characterisation of the planets is done using an open-source radiative transfer Python package, called petitRADTrans[3] (Mollière et al., 2019). The mixing ratios from the chemical kinetic code are converted into mass fractions, and used as input data for petitRADTrans. The default line absorbers are used (see Table 2 of Mollière et al. (2019) for references) and the spectra are calculated at low resolution ($\lambda/\Delta\lambda = 1000$). The Rayleigh scattering cross-sections for H_2 (Dalgarno and Williams, 1962) and He (Chan and Dalgarno, 1965) are considered, and we also add collision induced absorption (CIA) of the H_2–H_2 and H_2–He pairs (Richard et al., 2012). Note that when modelling the spectra, we exclude clouds. Including them can flatten the spectra (e.g. Ohno et al., 2020) due to the absorption and scattering of the UV-light.

3. Results

3.1. Thermal evolution

The thermal evolution of the planets can be seen in Fig. 1. The changes in T_{int} and T_{irr} can be seen in Figs. 2 and 3, respectively. The

[1] https://github.com/exoclime/VULCAN.
[2] https://github.com/exoclime/FastChem.
[3] https://petitradtrans.readthedocs.io/en/latest/.

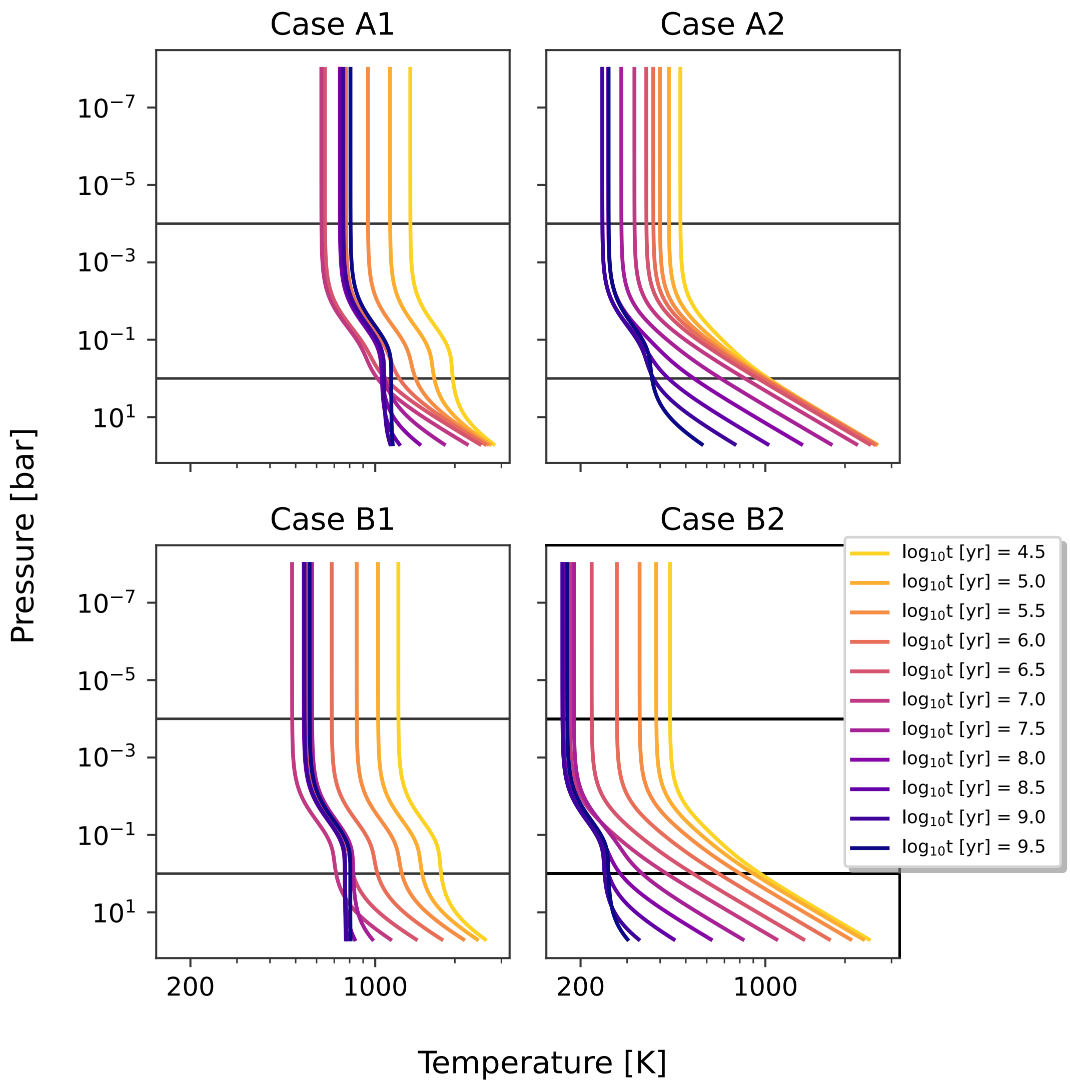

Fig. 1. The temperature–pressure (TP) profile of each planet. Darker colour indicates an older age as labelled. Black solid lines divide the upper, middle, and lower atmosphere as defined in Madhusudhan (2019). Note that the figures share both axes.

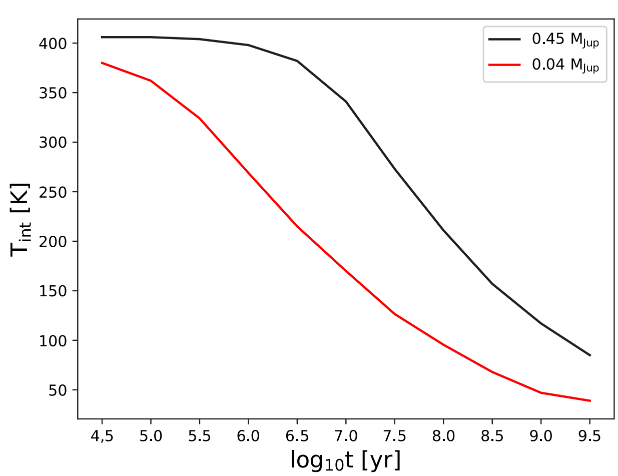

Fig. 2. The internal temperature as a function of the selected time steps. Black and red colours are the cases of the 0.45 M_{Jup} and 0.04 M_{Jup} planet, respectively.

Hertzsprung–Russell (H-R) diagram of the stars in the ages considered in this study is presented in Fig. 4. As expected, the planets radiate away their heat (e.g. Baraffe et al., 2003; Fortney et al., 2011), causing their internal temperature to decrease over time. A similar trend is visible in the planetary radii, R_p (Fig. 5). More massive planets take longer to cool down, which is also visible in Fig. 2. While the internal temperature of the 0.04 M_{Jup} planet shows a decreasing trend even in the first few thousand years (dropping from 380 K to 362 K between $10^{4.5}$ and 10^5 yr), the 0.45 M_{Jup} planet does not experience a significant cooling in the first 1 million year (stays at ∼406 K), however, in the following time steps its temperature keeps decreasing . The more massive planet (case A1 and case A2) has an internal temperature between 406 K and 85 K, whereas the internal temperature of the less massive planet (case B1 and case B2) ranges between 380 K and 39 K. The internal temperature ranges for the two planets are similar, but there are notable differences in the upper and lower bounds of the temperature ranges, hence the effect of high and low T_{int} can be investigated. The irradiation temperature, T_{irr}, is always the largest at earlier stages of the system, since after the formation of the system, both host stars are very luminous. As the stars follow the Hayashi-track their effective temperatures do not show a considerable change, but they experience a decrease in luminosity and hence the irradiation temperature of the planets are also decreasing, reaching its low-point when the system is around 10^7 yr old. Subsequently, the effective temperature of the host stars increases (i.e. T_{irr} starts to increase

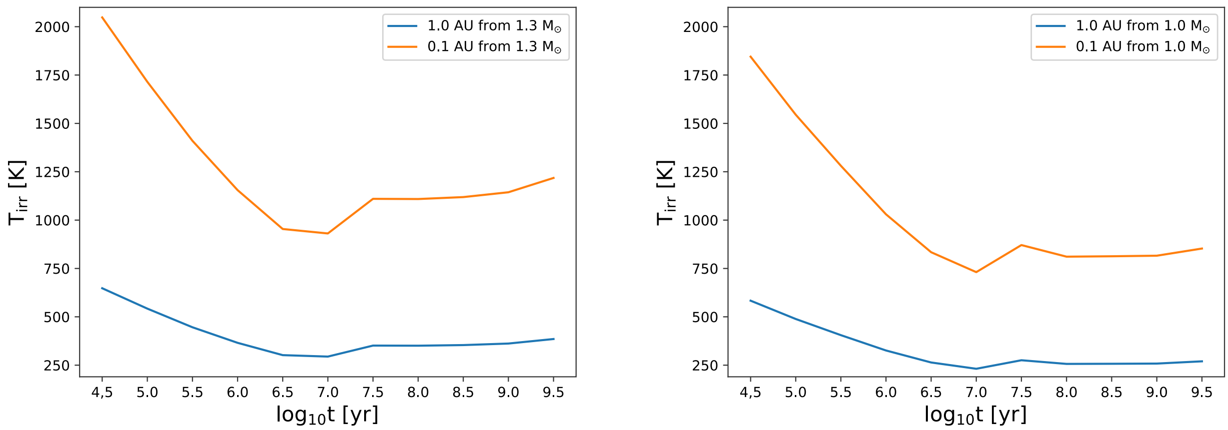

Fig. 3. Irradiation temperature as a function of age for the 1.3 $M_\odot$ (left panel) and 1.0 $M_\odot$ host star (right panel). Orange and blue colours indicate 0.1 and 1.0 AU distance, respectively.

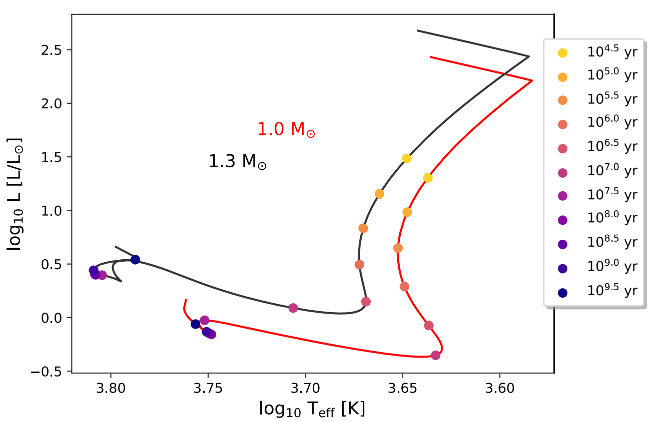

Fig. 4. The HR diagram of the 1.3 $M_\odot$ (black line) and 1.0 $M_\odot$ (red line) star. The individual dots represent the specific ages as labelled.

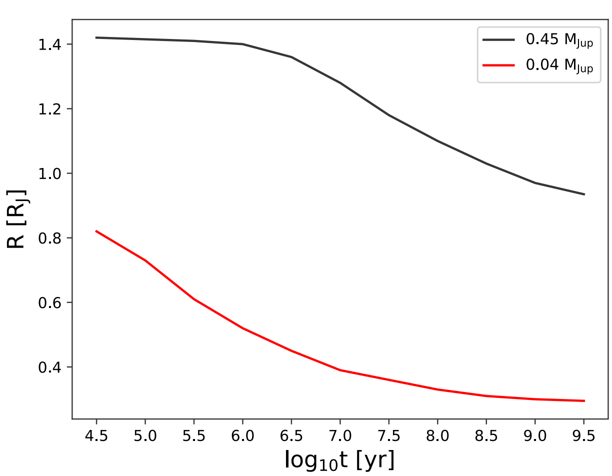

Fig. 5. The radius as a function of the selected time steps. Black and red colours are the cases of the 0.45 M_{Jup} and 0.04 M_{Jup} planet, respectively.

again) until the main-sequence phase is reached, at which both the luminosities and effective temperatures roughly remain constant.

Overall, the temperature–pressure profiles of the planets decrease with time. However, the temperature of the planetary atmosphere at 0.1 AU is increasing after 10^7 yr, especially in the intermediate and upper atmosphere. This is due to the increased incoming radiation from the host star as it reaches the main sequence phase. In the other cases, the planets are too far (i.e. $a = 1.0$ AU) to experience this upward trend.

3.2. Evolution of the composition

In the following subsections we compare the compositional evolution of case A1 with A2 (Section 3.2.1), and case B1 with B2 (Section 3.2.2). Figs. 6–9 show how the mixing ratio of some of the most important molecular species change with time for the different cases. The atmosphere is divided into three regions as shown in the figures with black lines. The upper atmosphere is below 10^{-4} bar, while the lower atmosphere is above 1 bar (Madhusudhan, 2019).

3.2.1. Cases A1 and A2

The most abundant species is H_2 in both cases, with exception of the early evolution ($<10^{4.5}$ yr) where the high incoming radiation from the host star causes atomic hydrogen to be dominant in the upper atmosphere for the short orbit period planet (A1). This is because the temperature is high enough (T ∼ 1400 K and T_{irr} ∼ 2000 K) for H_2 to dissociate. Although the relative abundance of H is much lower in the other atmospheric levels for both cases A1 and A2, the same decreasing trend is visible as the planet evolves and cools.

On the other hand, the $\mathbf{CO_2}$ mixing ratio is greatly affected by the thermal evolution of the planet as carbon prefers CO rather than CH_4 in hotter planets. CO_2 is CO and H_2O dependent. OH produced photochemically enhances the conversion of CO to CO_2 through the following reaction:

$$CO + OH \rightarrow CO_2 + H \tag{2}$$

where OH is produced by:

$$H_2O + H \rightarrow OH + H_2 \tag{3}$$

Hence, the net production is:

$$H_2O + CO \rightarrow CO_2 + H_2. \tag{4}$$

In case A1, the mixing ratio is largest in the middle and upper atmosphere between 10^6 – $10^{6.5}$ yr. In the upper atmosphere the relative abundance almost reaches $\sim 10^{-5}$, while in the intermediate and lower atmosphere it drops below to $\sim 10^{-7}$. At this point in time, the internal temperature of the planet starts to decrease as well (Fig. 2). After 10^6 yr, while the internal temperature of the planet decreases, the net change of the mixing ratio of CO_2 is negative in both cases. Due to the higher incoming radiation in case A1, the final mixing ratio in the upper atmosphere during this time is much higher compared to case A2. In case A1 it drops from $\sim 10^{-5}$ to $\sim 10^{-6}$ in the upper atmosphere,

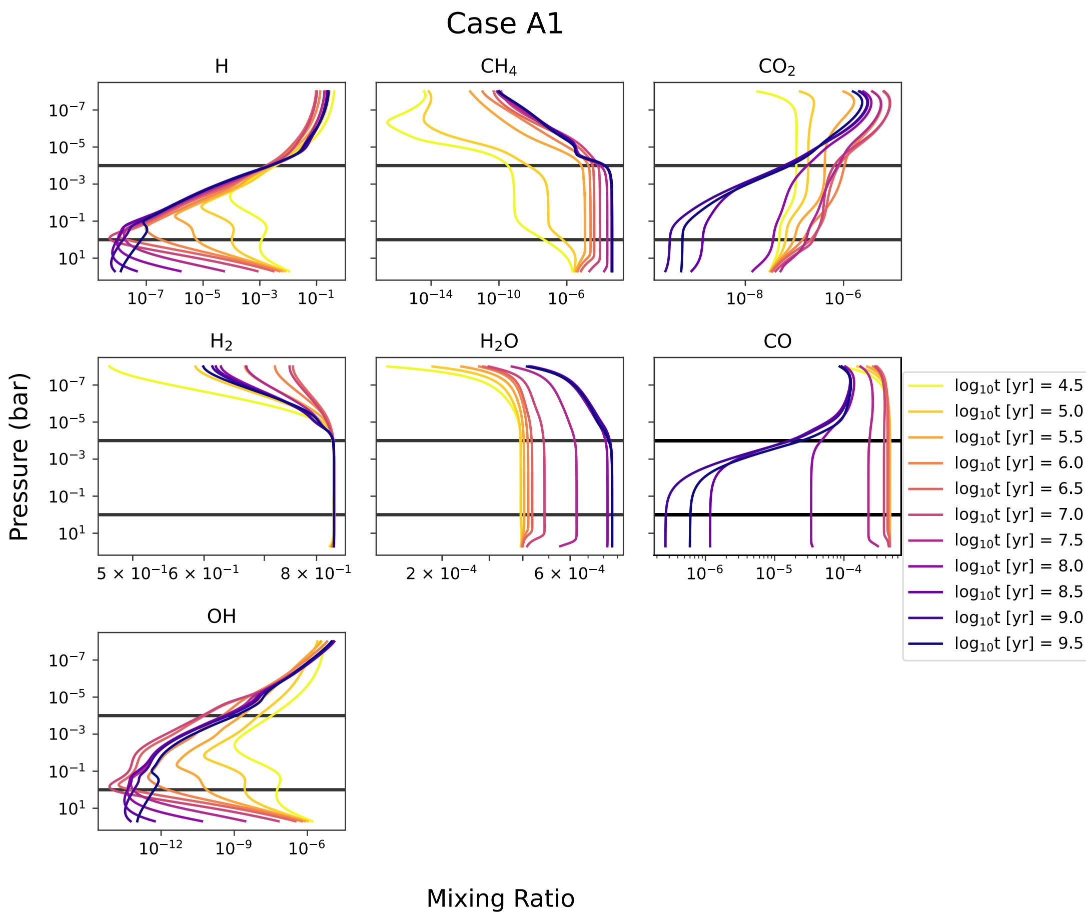

Fig. 6. The evolution of the mixing ratio of the most important species in case A1. Colourings are the same as in Fig. 1. Note that the range of the horizontal axes is different in the subplot of each species, whereas the vertical axes are shared.

while in case A2 it decreases from $\sim 2 \times 10^{-6}$ to $\sim 6 \times 10^{-8}$, reaching a minimum of $\sim 2 \times 10^{-10}$ at 10^9 year.

$\mathbf{H_2O}$ increases as the internal temperature decreases, and its mixing ratio is always within the 10^{-4} range, making it one of the most abundant species in the atmosphere throughout the evolution, irregardless of semi-major axis (Moses et al., 2013; Drummond et al., 2020; Zamyatina et al., 2023).

The mixing ratio of $\mathbf{CH_4}$ increases with age in both cases, as methane formation is favoured at lower temperatures (e.g., Moses et al. (2011)). In case A2, CH_4 becomes the primary carbon reservoir throughout the atmosphere after $10^{7.5}$ yr. In contrast, for case A1, CH_4 dominates over CO after the same period but is predominant only in the middle and lower atmosphere. This distinction highlights the significant influence of stellar radiation in the evolution. Additionally, it is notable that CO displays a trend opposite to that of CH_4, due to the preference of C to go to CH_4 or CO depending on the temperature (e.g., Moses et al., 2011).

3.2.2. Cases B1 and B2

Similarly to case A1, $\mathbf{H_2}$ is able to dissociate in the upper atmosphere of case B1 in the earlier stages of the evolution when the host star reaches the Hayashi-line, because of the high irradiation that leads to a high atmospheric temperature ($T \sim 1400$ K and $T_{irr} \sim 1800$ K).

In case B1, the mixing ratio of $\mathbf{CO_2}$ in the upper atmosphere shows an increasing trend from $\sim 10^{-7}$ to $\sim 2 \times 10^{-6}$ and it reaches $\sim 10^{-6}$ after the first million year, which is the effect of the incoming radiation, as in the other atmospheric levels, the CO_2 mixing ratio drops after a million years and reaching the minimum at 10^7 yr ($\sim 10^{-10}$). After 10^7 yr, the mixing ratio of CO_2 increases in case B1 in the middle and lower atmosphere, and in the later stages it reaches a mixing ratio of $\sim 10^{-7}$. During this period, the mixing ratio of methane drops slightly (less than 10 factor), which is the result of the $CH_4 \rightarrow CO$ net production. This can be due to the photolysis of $\mathbf{CH_4}$ and $\mathbf{H_2O}$ in the upper atmosphere, which triggers the **CO** production in lower pressure levels, however, CO is transported to the other atmospheric levels due to vertical mixing. Hotter atmosphere favours CO and hence CO_2, since they are linked kinetically, and this is the period when the atmospheric temperature of case B1 increases because the host star is in the main sequence phase and the irradiation increases. Our results also indicate when there is more CO and H_2O in the atmosphere, the CO_2 formation is more effective, therefore, larger CO_2 mixing ratio results in smaller CH_4 mixing ratio (Moses et al., 2011).

In contrast, in case B2, initially the mixing ratio of $\mathbf{CO_2}$ is $\sim 10^{-7}$ at all atmospheric levels, including the upper atmosphere, because it does not experience such incoming radiation. Then, as the planet cools, its mixing ratio shows a decreasing trend without significant fluctuations. Between 10^6 yr and 10^7 yr the factor of decrease is 10, whereas between 10^7 yr and $10^{9.5}$ yr it decreases almost by a factor of 20 and ends up with a value of $\sim 3 \times 10^{-10}$.

On the other hand, since cooler atmospheres favours methane, the mixing ratio of $\mathbf{CH_4}$ experiences an upward trend in case B2. Up to the first million year, its mixing ratio increases by a factor of 9. Then, between 10^6 yr and $10^{6.5}$ yr, the mixing ratio of CH_4 jumps to almost 4×10^{-4} and stays at this value. This is because the overall temperature of the atmosphere does not change drastically as well. Furthermore, in case B2, the mixing ratio of CH_4 is always larger than the mixing ratio of CO_2 in contrast to case B1, since in case B1 CH_4 only becomes more abundant in middle and lower atmospheric levels (due to stellar radiation) after 10^5 yr.

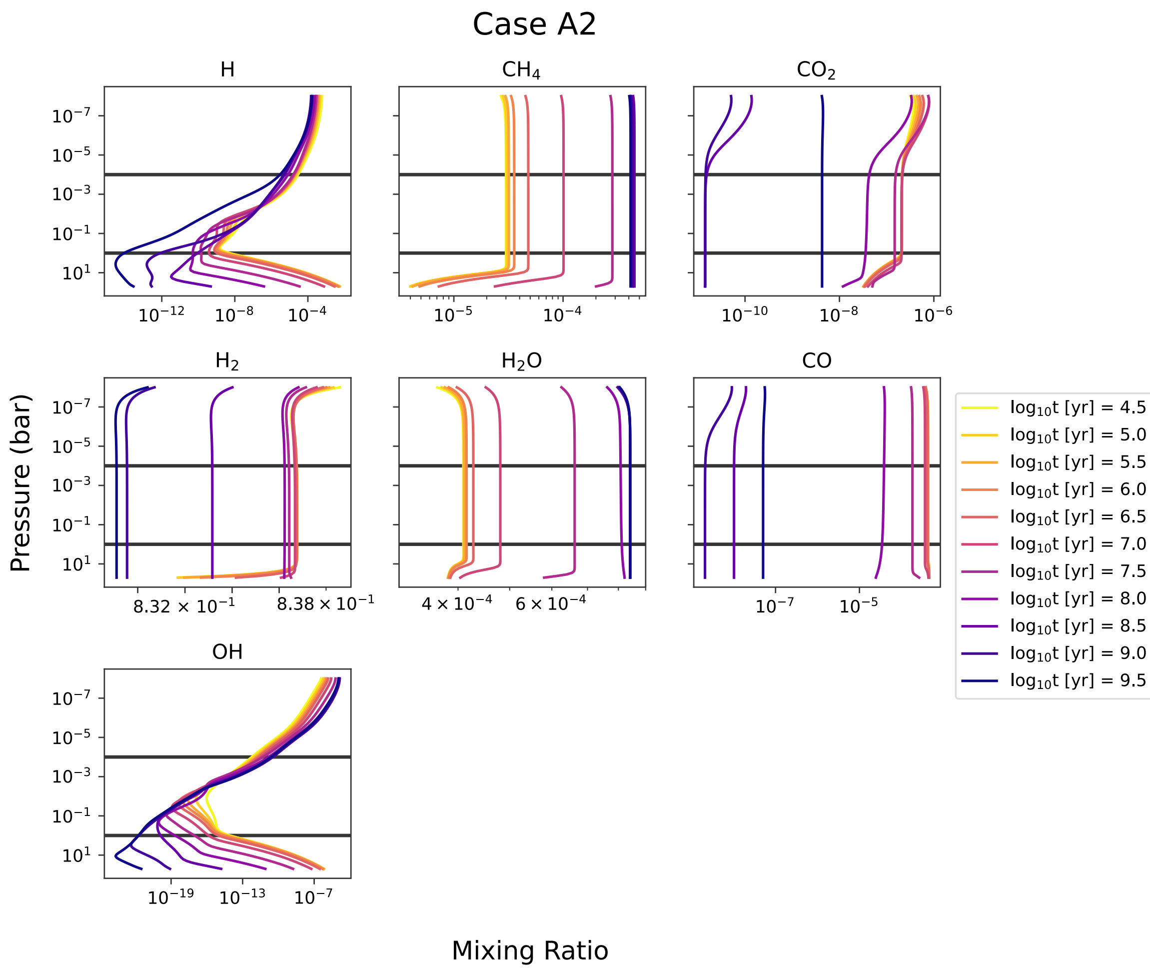

Fig. 7. Same as Fig. 6, but with case A2.

As discussed previously, $\mathbf{H_2O}$ remains stable at most temperature and pressure conditions. However, surprisingly, in case B2, the mixing ratio of water drops from $\sim10^{-3}$ to almost 10^{-5}, because the atmospheric temperature becomes so low at later stages (T < 300 K) that CH_4 becomes more dominant. This is because in case B2, the host star during the main-sequence experiences the low-point in its effective temperature, and the planet is further from the host star, which leads to much less OH in the atmosphere. OH is a crucial species in order to produce H_2O because of

$$OH + H_2 \rightarrow H_2O + H. \quad (5)$$

3.3. *Time-dependent features of the transmission spectra*

Motivated by JWST capabilities, we study the evolution of the transmission spectra from 0.6 μm and 10.0 μm of each planet (Fig. 10). The most important time-dependent features in every simulated planet that we found are the CH_4 (at ∼3.3 μm and ∼7.5 μm) and CO_2 (at ∼4.3 μm) peaks. H_2O also shapes the spectra considerably as it contributes to the total opacity the most, especially below 3.0 μm. The summary of the features in our simulated planets can be read in Table 2. In the following subsections we describe the spectra of the more massive (Section 3.3.1) and less massive (Section 3.3.2) planets. Note that in this paper we did not include Sulfur-bearing species in our calculations, but because of its relevance and recent detection in WASP-39 b (Feinstein et al., 2023; Alderson et al., 2023; Rustamkulov et al., 2023; Ahrer et al., 2023; Tsai et al., 2023; Powell et al., 2024) and WASP-107b (Dyrek et al., 2024), this will be further explored in future publications.

3.3.1. *Case A1 and A2*

On both cases (A1 and A2), at higher wavelengths (>1.5 μm), the transit radius decreases with time, mostly due to the evolution of the planets that drastically decrease their radius with time (Fig. 5). Besides the general trends on the depth of the transit, we also see differences in the spectral features with time.

A prominent, time-dependent feature is the CO_2 peak at ∼4.3 μm. It is visible until 10^8 yr in both cases and after that, methane overshadows this feature during the host star's main-sequence phase. This is related with the abundance of these species at different ages. We can see in Fig. 6, that the mixing ratio of CO_2 shows a gradual decrease with time in favour of methane. In addition, H_2O is also an important contributor to the opacity in the whole transmission spectra, and is one of the most abundant species in both cases at all times, which also helps overshadowing the carbon-dioxide feature. Fig. 11 (left panel) illustrates how the CO_2 feature changes with time. In case A1, this feature is largest at 10^6 yr with 210 ppm, whereas in case A2 the feature has a 125 ppm at $10^{4.5}$ yr, and then it shows a continuous decrease, in concordance with what is seen in the concentration of this species. Furthermore, at the last stage in case A2, the feature reappears with a size of only 33 ppm. Since the size of the observable feature fluctuates in case A1, it suggests that there might be a 'sweet spot' in which the CO_2 can be detected more easily in the atmosphere.

CH_4 produces features at ∼3.3 μm and ∼7.5 μm. While these are always visible in the colder case A2, it only appears after $10^{5.5}$ yr in case A1. Due to the extreme irradiation, the mixing ratio of methane is below 10^{-10} before $10^{5.5}$ yr, which is even lower in the upper atmosphere ($<10^{-12}$), hence water can easily overshadow the features

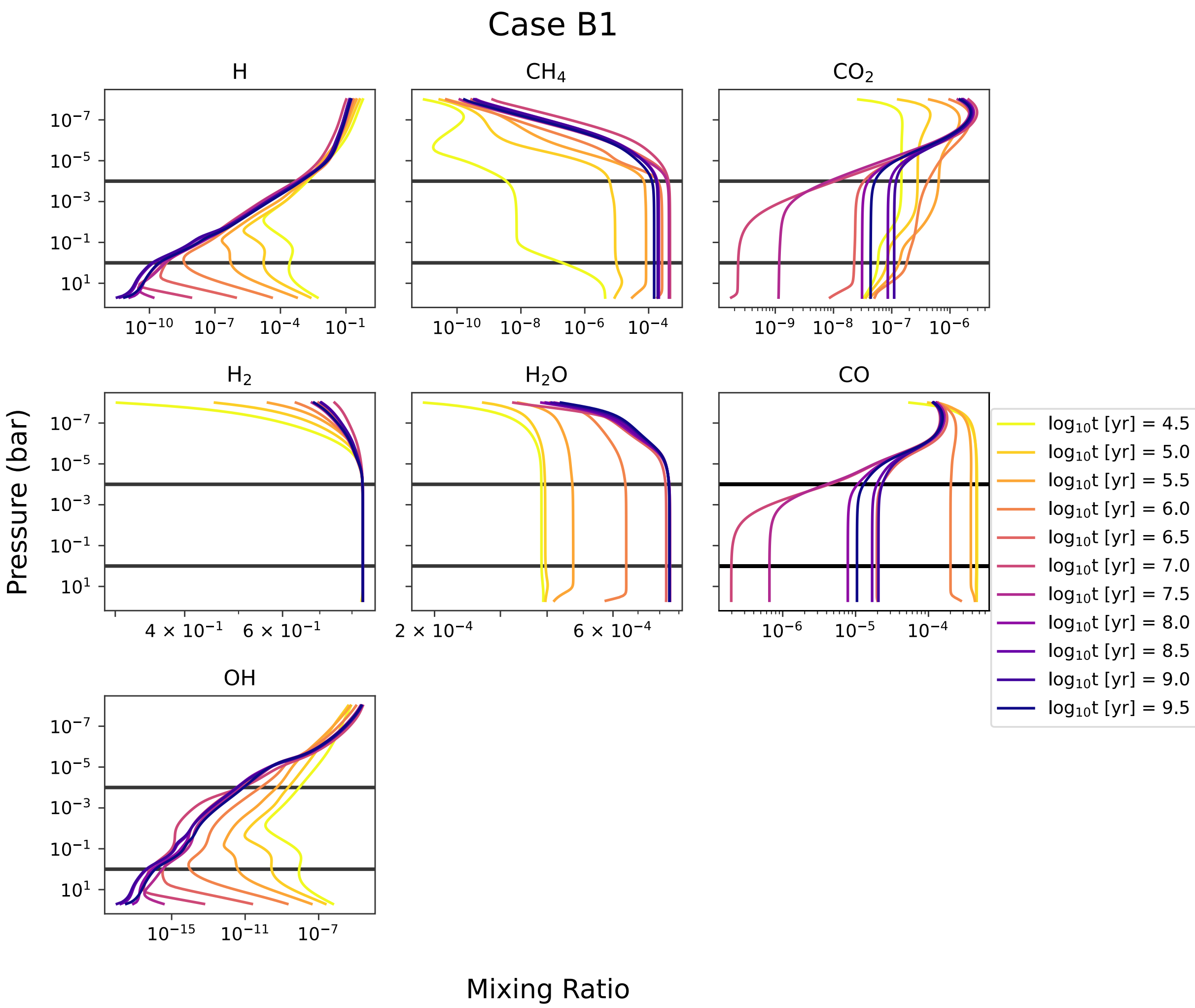

Fig. 8. Same as Fig. 6, but with case B1.

created by methane. These features are largest at later stages during the evolution of case A1, when the planet is cooler, with a peak size of 463 ppm and 229 ppm at 3.3 μm and 7.5 μm, respectively (see Table 2 and Fig. 11 middle and right panel). While the size of methane feature at shorter wavelength increases by more than a factor of 2 over time, the feature at longer wavelength does not experience a significant change during the evolution in case A1. In case A2, both CH_4 feature are largest at the beginning of the evolution with 218 ppm for the 3.3 μm feature and 127 ppm for the 7.5 μm feature. None of the features experience a gradual change over time as the planet cools in case A2 even though the mixing ratio of CH_4 increases by almost a factor of 10.

Even though the mixing ratio of H_2O is increasing with time in both cases, it mainly shapes the whole spectra until $10^{5.5}$ yr and after that, only the features at shorter wavelengths (<3 μm) are caused by water. Hence its contribution to the opacity at longer wavelengths is only large at temperature higher than 1000 K in every pressure level.

3.3.2. Case B1 and B2

The evolution of the transit radius is decreasing with time in both cases above ∼1.5 μm, while it is increasing below that wavelength range, similarly to case A1 and A2.

CO_2 behaves differently in the smaller planets compared to the larger planets. Since these planets become cooler faster, due to their smaller internal and irradiation temperatures, methane overshadows the CO_2 feature at 4.3 μm at younger ages (from 10^6 yr). However, this feature reappears after 10^8 yr in case B1, but its size is significantly smaller. While it is between around 250 ppm and 100 ppm until the first million years in case B1, this feature is less than 100 ppm when it reappears after 10^8 yr. Since the size of the feature does not show a continuous decline (see blue dotted line in Fig. 11), it also proves that the CO_2 feature has 'sweet spots' and visible with specific temperature and compositional combination. In case B2, the CO_2 feature is always smaller compared to case B1 as expected since it is a less irradiated planet, ranging from 110 ppm to 59 ppm. Based on the time when the CO_2 feature is largest in case B1 (Table 2 and left panel of Fig. 11), and the evolution of mixing ratio of CO_2 (Fig. 8), it becomes clear that the middle and lower atmosphere contributes to the feature.

Regarding the methane features, in case B1 they only become visible after $10^{5.5}$ yr, which is due to the high incoming radiation.

In case B2 they are always visible. The CH_4 features are largest before the first million years in both cases, reaching higher ppm than the ppm of CO_2 (see Table 2). Furthermore, the CH_4 features are always larger in the more irradiated planets, which is also seen in case A1 and A2 (Fig. 11), and in agreement with the mixing ratios observed.

4. Discussion

4.1. Limitation

Our study focuses on the chemical evolution of the atmospheres of four simulated gaseous planets and their observability due to the planetary and stellar evolution. A caveat in this study is the calculation

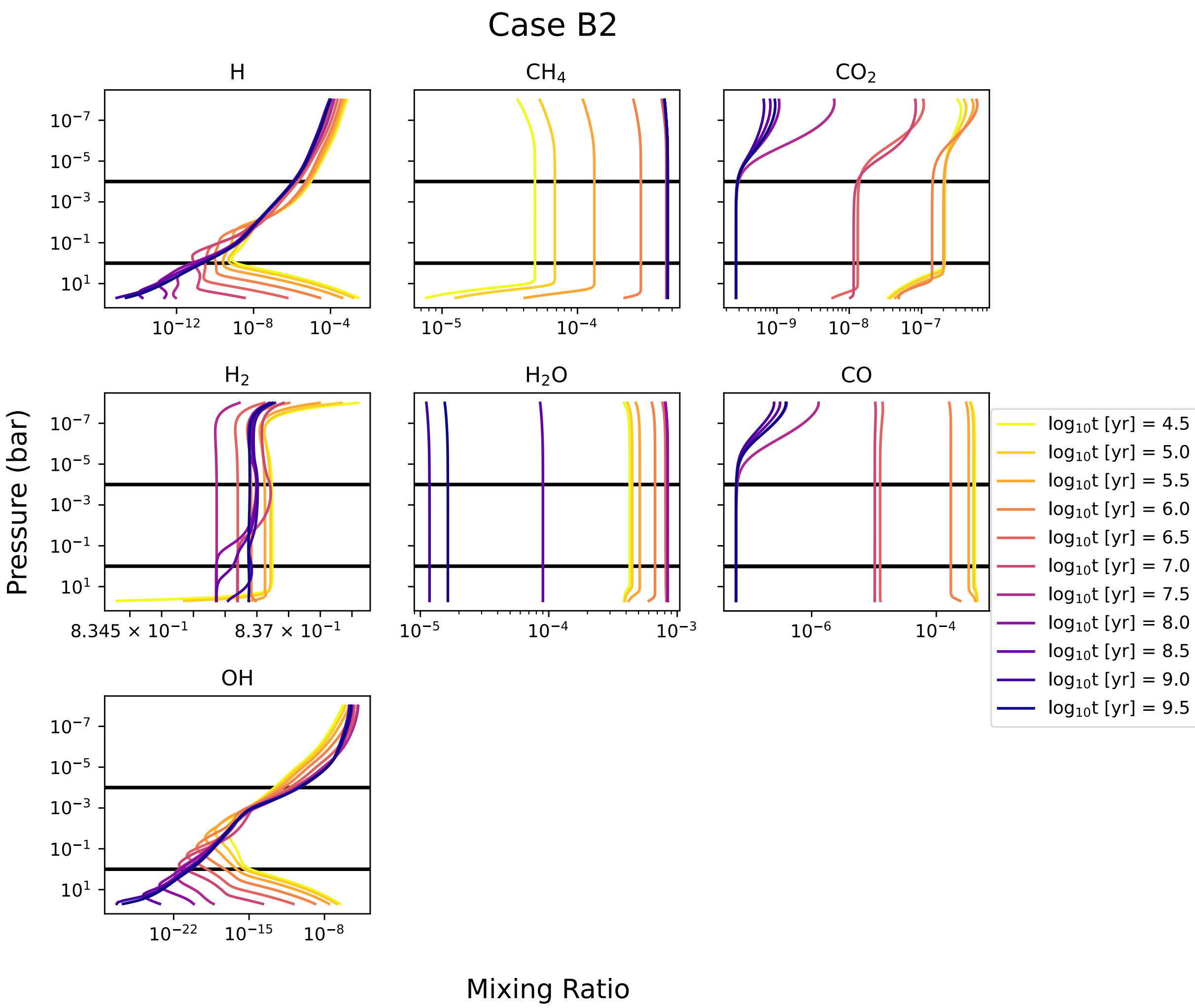

Fig. 9. Same as Fig. 6, but with case B2.

Table 2
Summary table of the most prominent time-dependent features in the transmission spectra of each planet. In the case of CH_4, the feature at ~3.3 μm and ~7.5 μm can be read without and with brackets, respectively.

	CO_2	Max ppm of CO_2	Time of max ppm of CO_2	CH_4	Max ppm of CH_4	Time of max ppm of CH_4
Case A1:	$\leq 10^{8.0}$ yr	210	$10^{6.0}$ yr	$\geq 10^{5.5}$ yr	463 (229)	$10^{9.5}$ yr ($10^{9.5}$ yr)
Case A2:	$\leq 10^{8.0}$ yr, $\geq 10^{9.5}$ yr	125	$10^{4.5}$ yr	Always	218 (127)	$10^{4.5}$ yr ($10^{4.5}$ yr)
Case B1:	$\leq 10^{6.0}$ yr, $\geq 10^{8.0}$ yr	252	$10^{4.5}$ yr	$\geq 10^{5.5}$ yr	710 (446)	$10^{5.5}$ yr ($10^{5.5}$ yr)
Case B2:	$\leq 10^{6.0}$ yr	110	$10^{4.5}$ yr	Always	243 (137)	$10^{4.5}$ yr ($10^{4.5}$ yr)

of the temperature–pressure profiles of the simulated planets, which is done with an analytical model by Heng et al. (2014). The model uses a two-stream approximation, which divides the radiation into two parts, i.e. as a pair of outgoing and incoming rays and hence simplifies the complex interactions of radiation with the atmosphere. Furthermore, it uses a characteristic longwave and shortwave opacity. In reality, opacities at different wavelengths influence the amount of radiation absorbed and emitted in the atmosphere. In regions where opacities are high, such as due to the presence of greenhouse gases (e.g. CO_2, H_2O, CH_4), more radiation is absorbed, leading to a higher temperature (e.g. Selsis et al., 2007).

In addition, throughout the whole evolution the spectra of the host stars are constant. This leads to another limitations as these stellar spectra are expected to be different especially at earlier stages, resulting in more UV flux and hence different atmospheric composition of the planets (Teal et al., 2022). However, when experimenting with the inclusion of the Sun's spectral evolution (Claire et al., 2012), it only had minor influence on the mixing ratios early in the evolution, i.e. when the Sun was in its maximal activity state. For this analysis, we used the results from case B2 at $t = 10^{5.5}$ yr as a starting point, updating only the Sun's spectra, scaled to 1.0 AU, at various timesteps. The only noticeable changes occurred in the mixing ratios of H and OH in the upper atmosphere. As solar activity diminished, there was a slight increase in both mixing ratios. Specifically, at pressure level of $\sim 10^{-7}$ bar, the mixing ratio of H increased from $\sim 3.12\times 10^{-5}$ to $\sim 8.32\times 10^{-5}$ between 0.3 Gyr and 3.9 Gyr. Similarly, the mixing ratio of OH rose from $\sim 1.24\times 10^{-10}$ to $\sim 3.59\times 10^{-10}$ over the same period. However, these changes did not affect the simulated transmission spectra. Hence, for simplicity, the spectra remained constant in this study.

Moreover, we exclude the incoming radiation when evolving the planets in MESA, and calculate the irradiation temperature separately.

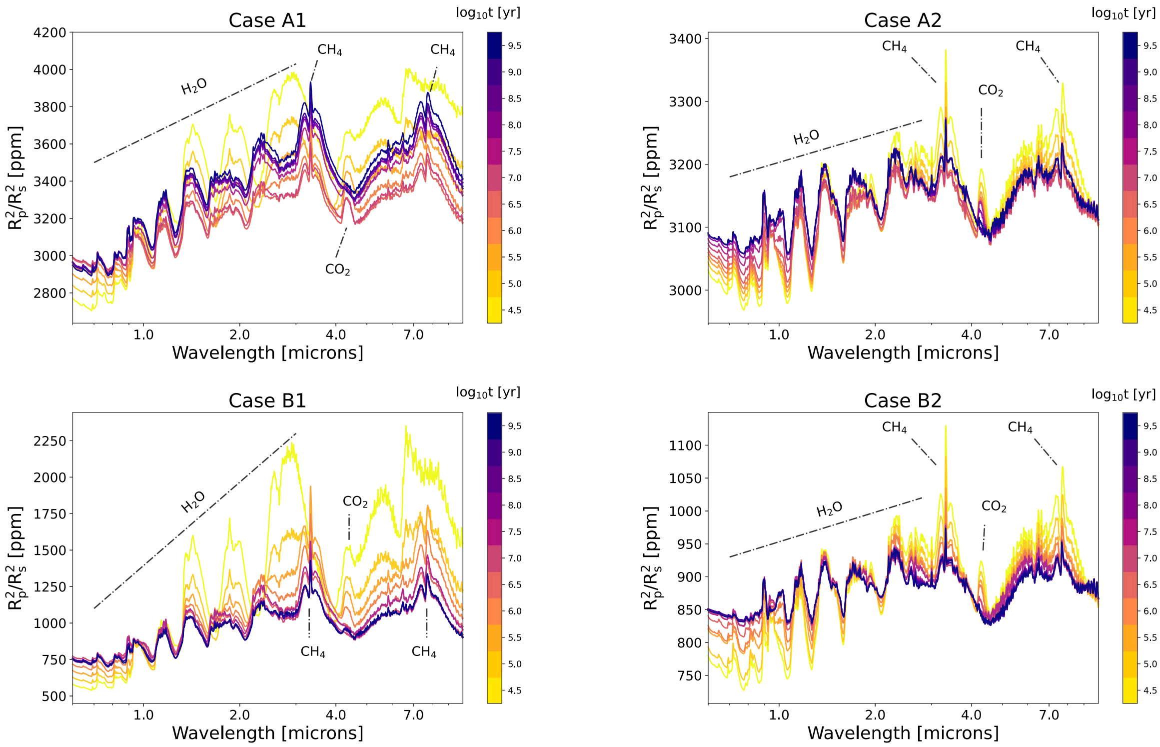

Fig. 10. The evolution of the transmission spectra of each planet. Darker colour indicates older stages, similarly as in Fig. 1. The most important molecular features are labelled with black. The spectra are convolved with a Gaussian filter to decrease resolution.

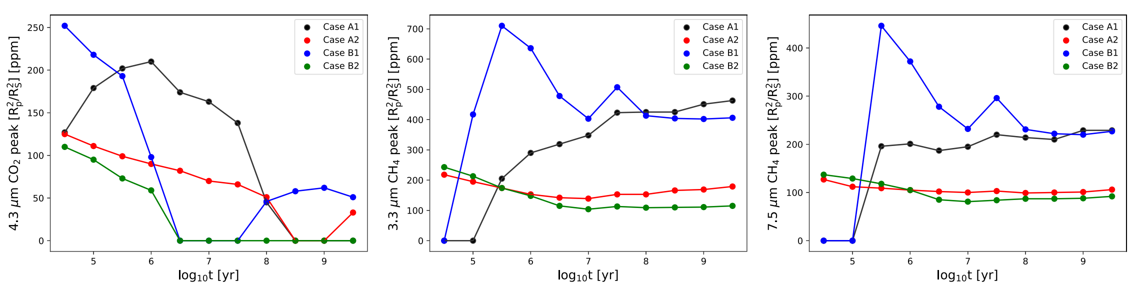

Fig. 11. The peak size of the CO_2 feature at ~4.3 μm (left panel), the CH_4 feature at ~3.3 (middle panel), and the CH_4 feature at ~7.5 (right panel) as the function of the selected time steps. Colours indicate the different cases as labelled.

This can have an impact on the radii of the planets, as the incoming radiation can inflate them, however, it was noted by the authors of Paxton et al. (2013) that this effect is mainly important if the semimajor axis is small (<0.1 AU).

Lastly, our study only dealt with transmission spectra, which provided a robust test case for examining changes in the atmospheric chemistry of gaseous planets. Emission spectra were not included in our current calculations but will be considered in future research.

5. Conclusion

In this study we simulated four different systems (Table 1) of varying masses and semi-major axes for $10^{9.5}$ yr by making use of the MESA evolutionary code and obtained the temperature–pressure profiles with a simple analytical approach that uses a two-stream approximation. Then, we modelled the change in composition with a photochemical kinetics code, VULCAN. The corresponding transmission spectra were obtained with the radiative transfer code petitRADTrans.

The change in composition (Figs. 6–9) driven by the thermal evolution (Fig. 1) of planets led to time-dependent features in their transmission spectra (Fig. 10). Our results showed that the species that change the most were CO_2 and CH_4. In summary, we found:

1. **CO_2** feature at ~4.3 μm was a prominent time-dependent feature in every planet's transmission spectra. In **case A1**, this feature was visible until 10^8 yr. It reached its maxima at 10^6 yr (210 ppm), then the feature's size decreased without fluctuations. In comparison, in **case A2** it lasted until 10^8 yr, however, its size showed a continuous decrease from the very beginning of the planet's evolution (from 125 ppm to 51 ppm). Based on our findings, the CO_2 feature is mainly affected by the evolution of the planet, that cools with time decreasing the amount of CO_2 in the atmosphere in favour of CH_4 and H_2O.
   In **case B1**, it was visible in the first one million years, and decreased in size without fluctuations after that (from 252 ppm to 98 ppm). In **case B2**, the CO_2 feature decreased from the beginning of the evolution (110 ppm) until 10^6 yr (59 ppm) without any fluctuations, similarly to cases A2 and B1. Additionally, in **case B1**, this feature reappeared after 10^8 yr with a much smaller peak size (~50–60 ppm) compared to the peak size at younger stages.
2. **CH_4** features at ~3.3 μm and ~7.5 μm were always visible in **case A2** and **case B2**. On the other hand, due to the high incoming radiation, these were not visible in the first million years of the planet's transmission spectra in **case A1** and **case B1**.

3. **H_2O** was an important contributor to the total opacity and in the first few thousand years, it shaped the whole spectra in **case A1** and **case B1**. After that, it only created the features below 3.0 μm. In **case A2** and **case B2**, water only shaped the spectra and provided features on it below 3.0 μm during the whole evolution, as these were less irradiated planets than the other two cases, hence other species, such as methane, could easily overshadow the water features on the longer wavelengths even at earlier stages of the planets.

Overall, our findings showed that both the planetary and stellar evolution affected the composition and hence observability of the atmosphere of H_2-dominated exoplanets, however, it should be noted that more research is needed covering a larger parameter space to gain a deeper insight into the evolution of exoplanetary atmospheres over a wider range of conditions. Based on our results the mixing ratio of CO_2 and CH_4 were sensitive to the thermal evolution and the features they create in the transmission spectra evolved with time. Therefore, by observing these different features in the future with the JWST we can better understand the formation and evolution of these exotic worlds.

CRediT authorship contribution statement

Viktória Kecskeméthy: Writing – original draft, Visualization, Validation, Methodology, Formal analysis, Conceptualization. **Amy Louca:** Writing – review & editing, Supervision, Conceptualization. **Yamila Miguel:** Writing – review & editing, Supervision, Conceptualization.

Declaration of competing interest

The authors declare that they have no known competing financial interests or personal relationships that could have appeared to influence the work reported in this paper.

Data availability

Data will be made available on request.

Acknowledgements

Y.M. acknowledges support from the European Research Council (ERC) under the European Union's Horizon 2020 research and innovation programme (grant agreement no. 101088557, N-GINE). The authors would like to thank the anonymous referee for the insightful comments and constructive feedback, which significantly improved the quality of this publication.

References

Ahrer, E.-M., Stevenson, K.B., Mansfield, M., Moran, S.E., Brande, J., Morello, G., Murray, C.A., Nikolov, N.K., Petit dit de la Roche, D.J.M., Schlawin, E., Wheatley, P.J., Zieba, S., Batalha, N.E., Damiano, M., Goyal, J.M., Lendl, M., Lothringer, J.D., Mukherjee, S., Ohno, K., Batalha, N.M., Battley, M.P., Bean, J.L., Beatty, T.G., Benneke, B., Berta-Thompson, Z.K., Carter, A.L., Cubillos, P.E., Daylan, T., Espinoza, N., Gao, P., Gibson, N.P., Gill, S., Harrington, J., Hu, R., Kreidberg, L., Lewis, N.K., Line, M.R., López-Morales, M., Parmentier, V., Powell, D.K., Sing, D.K., Tsai, S.-M., Wakeford, H.R., Welbanks, L., Alam, M.K., Alderson, L., Allen, N.H., Anderson, D.R., Barstow, J.K., Bayliss, D., Bell, T.J., Blecic, J., Bryant, E.M., Burleigh, M.R., Carone, L., Casewell, S.L., Changeat, Q., Chubb, K.L., Crossfield, I.J.M., Crouzet, N., Decin, L., Désert, J.-M., Feinstein, A.D., Flagg, L., Fortney, J.J., Gizis, J.E., Heng, K., Iro, N., Kempton, E.M.R., Kendrew, S., Kirk, J., Knutson, H.A., Komacek, T.D., Lagage, P.-O., Leconte, J., Lustig-Yaeger, J., MacDonald, R.J., Mancini, L., May, E.M., Mayne, N.J., Miguel, Y., Mikal-Evans, T., Molaverdikhani, K., Palle, E., Piaulet, C., Rackham, B.V., Redfield, S., Rogers, L.K., Roy, P.-A., Rustamkulov, Z., Shkolnik, E.L., Sotzen, K.S., Taylor, J., Tremblin, P., Tucker, G.S., Turner, J.D., de Val-Borro, M., Venot, O., Zhang, X., 2023. Early release science of the exoplanet WASP-39b with JWST NIRCam. Nature 614 (7949), 653–658. http://dx.doi.org/10.1038/s41586-022-05590-4.

Alderson, L., Wakeford, H.R., Alam, M.K., Batalha, N.E., Lothringer, J.D., Adams Redai, J., Barat, S., Brande, J., Damiano, M., Daylan, T., Espinoza, N., Flagg, L., Goyal, J.M., Grant, D., Hu, R., Inglis, J., Lee, E.K.H., Mikal-Evans, T., Ramos-Rosado, L., Roy, P.-A., Wallack, N.L., Batalha, N.M., Bean, J.L., Benneke, B., Berta-Thompson, Z.K., Carter, A.L., Changeat, Q., Colón, K.D., Crossfield, I.J.M., Désert, J.-M., Foreman-Mackey, D., Gibson, N.P., Kreidberg, L., Line, M.R., López-Morales, M., Molaverdikhani, K., Moran, S.E., Morello, G., Moses, J.I., Mukherjee, S., Schlawin, E., Sing, D.K., Stevenson, K.B., Taylor, J., Aggarwal, K., Ahrer, E.-M., Allen, N.H., Barstow, J.K., Bell, T.J., Blecic, J., Casewell, S.L., Chubb, K.L., Crouzet, N., Cubillos, P.E., Decin, L., Feinstein, A.D., Fortney, J.J., Harrington, J., Heng, K., Iro, N., Kempton, E.M.-R., Kirk, J., Knutson, H.A., Krick, J., Leconte, J., Lendl, M., MacDonald, R.J., Mancini, L., Mansfield, M., May, E.M., Mayne, N.J., Miguel, Y., Nikolov, N.K., Ohno, K., Palle, E., Parmentier, V., Petit dit de la Roche, D.J.M., Piaulet, C., Powell, D., Rackham, B.V., Redfield, S., Rogers, L.K., Rustamkulov, Z., Tan, X., Tremblin, P., Tsai, S.-M., Turner, J.D., de Val-Borro, M., Venot, O., Welbanks, L., Wheatley, P.J., Zhang, X., 2023. Early release science of the exoplanet WASP-39b with JWST NIRSpec G395H. Nature 614 (7949), 664–669. http://dx.doi.org/10.1038/s41586-022-05591-3.

Baraffe, I., Chabrier, G., Barman, T.S., Allard, F., Hauschildt, P.H., 2003. Evolutionary models for cool brown dwarfs and extrasolar giant planets. The case of HD 209458. Astron. Astrophys. 402, 701–712. http://dx.doi.org/10.1051/0004-6361:20030252.

Birkmann, S.M., Ferruit, P., Giardino, G., Nielsen, L.D., García Muñoz, A., Kendrew, S., Rauscher, B.J., Beck, T.L., Keyes, C., Valenti, J.A., Jakobsen, P., Dorner, B., Alves de Oliveira, C., Arribas, S., Böker, T., Bunker, A.J., Charlot, S., de Marchi, G., Kumari, N., López-Caniego, M., Lützgendorf, N., Maiolino, R., Manjavacas, E., Marston, A., Moseley, S.H., Prizkal, N., Proffitt, C., Rawle, T., Rix, H.-W., te Plate, M., Sabbi, E., Sirianni, M., Willott, C.J., Zeidler, P., 2022. The near-infrared spectrograph (NIRSpec) on the james webb space telescope. IV. Capabilities and predicted performance for exoplanet characterization. Astron. Astrophys. 661, A83. http://dx.doi.org/10.1051/0004-6361/202142592, arXiv:2202.03309.

Carter, A.L., Hinkley, S., Kammerer, J., Skemer, A., Biller, B.A., Leisenring, J.M., Millar-Blanchaer, M.A., Petrus, S., Stone, J.M., Ward-Duong, K., Wang, J.J., Girard, J.H., Hines, D.C., Perrin, M.D., Pueyo, L., Balmer, W.O., Bonavita, M., Bonnefoy, M., Chauvin, G., Choquet, E., Christiaens, V., Danielski, C., Kennedy, G.M., Matthews, E.C., Miles, B.E., Patapis, P., Ray, S., Rickman, E., Sallum, S., Stapelfeldt, K.R., Whiteford, N., Zhou, Y., Absil, O., Boccaletti, A., Booth, M., Bowler, B.P., Chen, C.H., Currie, T., Fortney, J.J., Grady, C.A., Greebaum, A.Z., Henning, T., Hoch, K.K.W., Janson, M., Kalas, P., Kenworthy, M.A., Kervella, P., Kraus, A.L., Lagage, P.-O., Liu, M.C., Macintosh, B., Marino, S., Marley, M.S., Marois, C., Matthews, B.C., Mawet, D., McElwain, M.W., Metchev, S., Meyer, M.R., Molliere, P., Moran, S.E., Morley, C.V., Mukherjee, S., Pantin, E., Quirrenbach, A., Rebollido, I., Ren, B.B., Schneider, G., Vasist, M., Worthen, K., Wyatt, M.C., Briesemeister, Z.W., Bryan, M.L., Calissendorff, P., Cantalloube, F., Cugno, G., De Furio, M., Dupuy, T.J., Factor, S.M., Faherty, J.K., Fitzgerald, M.P., Franson, K., Gonzales, E.C., Hood, C.E., Howe, A.R., Kuzuhara, M., Lagrange, A.-M., Lawson, K., Lazzoni, C., Lew, B.W.P., Liu, P., Llop-Sayson, J., Lloyd, J.P., Martinez, R.A., Mazoyer, J., Palma-Bifani, P., Quanz, S.P., Redai, J.A., Samland, M., Schlieder, J.E., Tamura, M., Tan, X., Uyama, T., Vigan, A., Vos, J.M., Wagner, K., Wolff, S.G., Ygouf, M., Zhang, X., Zhang, K., Zhang, Z., 2023. The JWST early release science program for direct observations of exoplanetary systems I: High-contrast imaging of the exoplanet HIP 65426 b from 2 to 16 μm. ApJ Lett. 951 (1), L20. http://dx.doi.org/10.3847/2041-8213/acd93e.

Chan, Y.M., Dalgarno, A., 1965. The refractive index of helium. Proc. Phys. Soc. 85 (2), 227–230. http://dx.doi.org/10.1088/0370-1328/85/2/304.

Claire, M.W., Sheets, J., Cohen, M., Ribas, I., Meadows, V.S., Catling, D.C., 2012. The evolution of solar flux from 0.1 nm to 160 μm: Quantitative estimates for planetary studies. Astrophys. J. 757 (1), 95. http://dx.doi.org/10.1088/0004-637X/757/1/95.

Dalgarno, A., Williams, D.A., 1962. Rayleigh scattering by molecular hydrogen. Astrophys. J. 136, 690–692. http://dx.doi.org/10.1086/147428.

Drummond, B., Hébrard, E., Mayne, N.J., Venot, O., Ridgway, R.J., Changeat, Q., Tsai, S.-M., Manners, J., Tremblin, P., Abraham, N.L., Sing, D., Kohary, K., 2020. Implications of three-dimensional chemical transport in hot jupiter atmospheres: Results from a consistently coupled chemistry-radiation-hydrodynamics model. Astron. Astrophys. 636, A68. http://dx.doi.org/10.1051/0004-6361/201937153.

Drummond, B., Tremblin, P., Baraffe, I., Amundsen, D.S., Mayne, N.J., Venot, O., Goyal, J., 2016. The effects of consistent chemical kinetics calculations on the pressure-temperature profiles and emission spectra of hot jupiters. Astron. Astrophys. 594, A69. http://dx.doi.org/10.1051/0004-6361/201628799.

Dyrek, A., Min, M., Decin, L., Bouwman, J., Crouzet, N., Mollière, P., Lagage, P.-O., Konings, T., Tremblin, P., Güdel, M., Pye, J., Waters, R., Henning, T., Vandenbussche, B., Ardevol Martinez, F., Argyriou, I., Ducrot, E., Heinke, L., van Looveren, G., Absil, O., Barrado, D., Baudoz, P., Boccaletti, A., Cossou, C., Coulais, A., Edwards, B., Gastaud, R., Glasse, A., Glauser, A., Greene, T.P., Kendrew, S., Krause, O., Lahuis, F., Mueller, M., Olofsson, G., Patapis, P., Rouan, D., Royer, P., Scheithauer, S., Waldmann, I., Whiteford, N., Colina, L., van Dishoeck, E.F., Östlin, G., Ray, T.P., Wright, G., 2024. SO_2, silicate clouds, but no CH_4 detected in a warm neptune. Nature 625 (7993), 51–54. http://dx.doi.org/10.1038/s41586-023-06849-0, arXiv:2311.12515.

Fauchez, T.J., Villanueva, G.L., Sergeev, D.E., Turbet, M., Boutle, I.A., Tsigaridis, K., Way, M.J., Wolf, E.T., Domagal-Goldman, S.D., Forget, F., Haqq-Misra, J., Kopparapu, R.K., Manners, J., Mayne, N.J., 2022. The TRAPPIST-1 habitable atmosphere intercomparison (THAI). III. Simulated observables—the return of the spectrum. Planet. Sci. J. 3 (9), 213. http://dx.doi.org/10.3847/PSJ/ac6cf1.

Feinstein, A.D., Radica, M., Welbanks, L., Murray, C.A., Ohno, K., Coulombe, L.-P., Espinoza, N., Bean, J.L., Teske, J.K., Benneke, B., Line, M.R., Rustamkulov, Z., Saba, A., Tsiaras, A., Barstow, J.K., Fortney, J.J., Gao, P., Knutson, H.A., MacDonald, R.J., Mikal-Evans, T., Rackham, B.V., Taylor, J., Parmentier, V., Batalha, N.M., Berta-Thompson, Z.K., Carter, A.L., Changeat, Q., dos Santos, L.A., Gibson, N.P., Goyal, J.M., Kreidberg, L., López-Morales, M., Lothringer, J.D., Miguel, Y., Molaverdikhani, K., Moran, S.E., Morello, G., Mukherjee, S., Sing, D.K., Stevenson, K.B., Wakeford, H.R., Ahrer, E.-M., Alam, M.K., Alderson, L., Allen, N.H., Batalha, N.E., Bell, T.J., Blecic, J., Brande, J., Caceres, C., Casewell, S.L., Chubb, K.L., Crossfield, I.J.M., Crouzet, N., Cubillos, P.E., Decin, L., Désert, J.-M., Harrington, J., Heng, K., Henning, T., Iro, N., Kempton, E.M.-R., Kendrew, S., Kirk, J., Krick, J., Lagage, P.-O., Lendl, M., Mancini, L., Mansfield, M., May, E.M., Mayne, N.J., Nikolov, N.K., Palle, E., Petit dit de la Roche, D.J.M., Piaulet, C., Powell, D., Redfield, S., Rogers, L.K., Roman, M.T., Roy, P.-A., Nixon, M.C., Schlawin, E., Tan, X., Tremblin, P., Turner, J.D., Venot, O., Waalkes, W.C., Wheatley, P.J., Zhang, X., 2023. Early release science of the exoplanet WASP-39b with JWST NIRISS. Nature 614 (7949), 670–675. http://dx.doi.org/10.1038/s41586-022-05674-1.

Fortney, J.J., Ikoma, M., Nettelmann, N., Guillot, T., Marley, M.S., 2011. Self-consistent model atmospheres and the cooling of the solar system's giant planets. Astrophys. J. 729 (1), 32.

Gueymard, C.A., 2018. Revised composite extraterrestrial spectrum based on recent solar irradiance observations. Sol. Energy 169, 434–440. http://dx.doi.org/10.1016/j.solener.2018.04.067, URL: https://www.sciencedirect.com/science/article/pii/S0038092X1830433X.

Guillot, T., 2010. On the radiative equilibrium of irradiated planetary atmospheres. Astron. Astrophys. 520, A27. http://dx.doi.org/10.1051/0004-6361/200913396.

Heng, K., Mendonça, J.M., Lee, J.-M., 2014. Analytical models of exoplanetary atmospheres. II. Radiative transfer via the two-stream approximation. Astrophys. J. Suppl. Ser. 215 (1), 4. http://dx.doi.org/10.1088/0067-0049/215/1/4.

Hobbs, R., Shorttle, O., Madhusudhan, N., Rimmer, P., 2019. A chemical kinetics code for modelling exoplanetary atmospheres. Mon. Not. R. Astron. Soc. 487 (2), 2242–2261.

Husser, T.-O., von Berg, S.W., Dreizler, S., Homeier, D., Reiners, A., Barman, T., Hauschildt, P.H., 2013. A new extensive library of PHOENIX stellar atmospheres and synthetic spectra. Astron. Astrophys. 553, A6. http://dx.doi.org/10.1051/0004-6361/201219058.

JWST Transiting Exoplanet Community Early Release Science Team, Ahrer, E.-M., Alderson, L., Batalha, N.M., Batalha, N.E., Bean, J.L., Beatty, T.G., Bell, T.J., Benneke, B., Berta-Thompson, Z.K., Carter, A.L., Crossfield, I.J.M., Espinoza, N., Feinstein, A.D., Fortney, J.J., Gibson, N.P., Goyal, J.M., Kempton, E.M.-R., Kirk, J., Kreidberg, L., López-Morales, M., Line, M.R., Lothringer, J.D., Moran, S.E., Mukherjee, S., Ohno, K., Parmentier, V., Piaulet, C., Rustamkulov, Z., Schlawin, E., Sing, D.K., Stevenson, K.B., Wakeford, H.R., Allen, N.H., Birkmann, S.M., Brande, J., Crouzet, N., Cubillos, P.E., Damiano, M., Désert, J.-M., Gao, P., Harrington, J., Hu, R., Kendrew, S., Knutson, H.A., Lagage, P.-O., Leconte, J., Lendl, M., MacDonald, R.J., May, E.M., Miguel, Y., Molaverdikhani, K., Moses, J.I., Murray, C.A., Nehring, M., Nikolov, N.K., Petit dit de la Roche, D.J.M., Radica, M., Roy, P.-A., Stassun, K.G., Taylor, J., Waalkes, W.C., Wachiraphan, P., Welbanks, L., Wheatley, P.J., Aggarwal, K., Alam, M.K., Banerjee, A., Barstow, J.K., Blecic, J., Casewell, S.L., Changeat, Q., Chubb, K.L., Colón, K.D., Coulombe, L.-P., Daylan, T., de Val-Borro, M., Decin, L., Dos Santos, L.A., Flagg, L., France, K., Fu, G., García Muñoz, A., Gizis, J.E., Glidden, A., Grant, D., Heng, K., Henning, T., Hong, Y.-C., Inglis, J., Iro, N., Kataria, T., Komacek, T.D., Krick, J.E., Lee, E.K.H., Lewis, N.K., Lillo-Box, J., Lustig-Yaeger, J., Mancini, L., Mandell, A.M., Mansfield, M., Marley, M.S., Mikal-Evans, T., Morello, G., Nixon, M.C., Ortiz Ceballos, K., Piette, A.A.A., Powell, D., Rackham, B.V., Ramos-Rosado, L., Rauscher, E., Redfield, S., Rogers, L.K., Roman, M.T., Roudier, G.M., Scarsdale, N., Shkolnik, E.L., Southworth, J., Spake, J.J., Steinrueck, M.E., Tan, X., Teske, J.K., Tremblin, P., Tsai, S.-M., Tucker, G.S., Turner, J.D., Valenti, J.A., Venot, O., Waldmann, I.P., Wallack, N.L., Zhang, X., Zieba, S., 2023. Identification of carbon dioxide in an exoplanet atmosphere. Nature 614 (7949), 649–652. http://dx.doi.org/10.1038/s41586-022-05269-w.

Lodders, K., Fegley, B., 2002. Atmospheric chemistry in giant planets, brown dwarfs, and low-mass dwarf stars. I. Carbon, nitrogen, and oxygen. Icarus 155 (2), 393–424. http://dx.doi.org/10.1006/icar.2001.6740.

Lodders, K., Palme, H., Gail, H.-P., 2009. Abundances of the elements in the solar system. Landolt Bornstein 4B, 712. http://dx.doi.org/10.1007/978-3-540-88055-4_34.

Madhusudhan, N., 2019. Exoplanetary atmospheres: Key insights, challenges, and prospects. Annu. Rev. Astron. Astrophys. 57, 617–663. http://dx.doi.org/10.1146/annurev-astro-081817-051846, arXiv:1904.03190.

Miguel, Y., Kaltenegger, L., 2014. Exploring atmospheres of hot mini-neptunes and extrasolar giant planets orbiting different stars with application to HD 97658b, WASP-12b, CoRoT-2b, XO-1b, and HD 189733b. Astrophys. J. 780 (2), 166. http://dx.doi.org/10.1088/0004-637X/780/2/166, arXiv:1311.0201.

Mollière, P., Wardenier, J.P., van Boekel, R., Henning, T., Molaverdikhani, K., Snellen, I.A.G., 2019. petitRADTRANS. Astron. Astrophys. 627, A67. http://dx.doi.org/10.1051/0004-6361/201935470.

Moses, J.I., Madhusudhan, N., Visscher, C., Freedman, R.S., 2013. Chemical consequences of the C/O ratio on hot jupiters: Examples from WASP-12b, CoRoT-2b, XO-1b, and HD 189733b. Astrophys. J. 763 (1), 25.

Moses, J.I., Visscher, C., Fortney, J.J., Showman, A.P., Lewis, N.K., Griffith, C.A., Klippenstein, S.J., Shabram, M., Friedson, A.J., Marley, M.S., Freedman, R.S., 2011. Disequilibrium carbon, oxygen, and nitrogen chemistry in the atmospheres of HD 189733b and HD 209458b. Astrophys. J. 737 (1), 15.

Ohno, K., Okuzumi, S., Tazaki, R., 2020. Clouds of fluffy aggregates: How they form in exoplanetary atmospheres and influence transmission spectra. Astrophys. J. 891 (2), 131.

Parmentier, V., Showman, A.P., Lian, Y., 2013. 3D mixing in hot jupiters atmospheres. I. Application to the day/night cold trap in HD 209458b. Astron. Astrophys. 558, A91.

Paxton, B., Bildsten, L., Dotter, A., Herwig, F., Lesaffre, P., Timmes, F., 2010. Modules for experiments in stellar astrophysics (MESA). Astrophys. J. Suppl. Ser. 192 (1), 3. http://dx.doi.org/10.1088/0067-0049/192/1/3.

Paxton, B., Cantiello, M., Arras, P., Bildsten, L., Brown, E.F., Dotter, A., Mankovich, C., Montgomery, M.H., Stello, D., Timmes, F.X., Townsend, R., 2013. Modules for experiments in stellar astrophysics (MESA): Planets, oscillations, rotation, and massive stars. Astrophys. J. Suppl. Ser. 208 (1), 4. http://dx.doi.org/10.1088/0067-0049/208/1/4.

Powell, D., Feinstein, A.D., Lee, E.K.H., Zhang, M., Tsai, S.-M., Taylor, J., Kirk, J., Bell, T., Barstow, J.K., Gao, P., Bean, J.L., Blecic, J., Chubb, K.L., Crossfield, I.J.M., Jordan, S., Kitzmann, D., Moran, S.E., Morello, G., Moses, J.I., Welbanks, L., Yang, J., Zhang, X., Ahrer, E.-M., Bello-Arufe, A., Brande, J., Casewell, S.L., Crouzet, N., Cubillos, P.E., Demory, B.-O., Dyrek, A., Flagg, L., Hu, R., Inglis, J., Jones, K.D., Kreidberg, L., López-Morales, M., Lagage, P.-O., Meier Valdés, E.A., Miguel, Y., Parmentier, V., Piette, A.A.A., Rackham, B.V., Radica, M., Redfield, S., Stevenson, K.B., Wakeford, H.R., Aggarwal, K., Alam, M.K., Batalha, N.M., Batalha, N.E., Benneke, B., Berta-Thompson, Z.K., Brady, R.P., Caceres, C., Carter, A.L., Désert, J.-M., Harrington, J., Iro, N., Line, M.R., Lothringer, J.D., MacDonald, R.J., Mancini, L., Molaverdikhani, K., Mukherjee, S., Nixon, M.C., Oza, A.V., Palle, E., Rustamkulov, Z., Sing, D.K., Steinrueck, M.E., Venot, O., Wheatley, P.J., Yurchenko, S.N., 2024. Sulfur dioxide in the mid-infrared transmission spectrum of WASP-39b. Nature 626 (8001), 979–983. http://dx.doi.org/10.1038/s41586-024-07040-9.

Richard, C., Gordon, I.E., Rothman, L.S., Abel, M., Frommhold, L., Gustafsson, M., Hartmann, J.-M., Hermans, C., Lafferty, W.J., Orton, G.S., Smith, K.M., Tran, H., 2012. New section of the HITRAN database: Collision-induced absorption (CIA). J. Quant. Spectrosc. Radiat. Transfer 113 (11), 1276–1285. http://dx.doi.org/10.1016/j.jqsrt.2011.11.004.

Rimmer, P.B., Helling, C., 2016. A chemical kinetics network for lightning and life in planetary atmospheres. Astrophys. J. Suppl. 224 (1), 9. http://dx.doi.org/10.3847/0067-0049/224/1/9.

Rustamkulov, Z., Sing, D.K., Mukherjee, S., May, E.M., Kirk, J., Schlawin, E., Line, M.R., Piaulet, C., Carter, A.L., Batalha, N.E., Goyal, J.M., López-Morales, M., Lothringer, J.D., MacDonald, R.J., Moran, S.E., Stevenson, K.B., Wakeford, H.R., Espinoza, N., Bean, J.L., Batalha, N.M., Benneke, B., Berta-Thompson, Z.K., Crossfield, I.J.M., Gao, P., Kreidberg, L., Powell, D.K., Cubillos, P.E., Gibson, N.P., Leconte, J., Molaverdikhani, K., Nikolov, N.K., Parmentier, V., Roy, P., Taylor, J., Turner, J.D., Wheatley, P.J., Aggarwal, K., Ahrer, E., Alam, M.K., Alderson, L., Allen, N.H., Banerjee, A., Barat, S., Barrado, D., Barstow, J.K., Bell, T.J., Blecic, J., Brande, J., Casewell, S., Changeat, Q., Chubb, K.L., Crouzet, N., Daylan, T., Decin, L., Désert, J., Mikal-Evans, T., Feinstein, A.D., Flagg, L., Fortney, J.J., Harrington, J., Heng, K., Hong, Y., Hu, R., Iro, N., Kataria, T., Kempton, E.M.-R., Krick, J., Lendl, M., Lillo-Box, J., Louca, A., Lustig-Yaeger, J., Mancini, L., Mansfield, M., Mayne, N.J., Miguel, Y., Morello, G., Ohno, K., Palle, E., Petit dit de la Roche, D.J.M., Rackham, B.V., Radica, M., Ramos-Rosado, L., Redfield, S., Rogers, L.K., Shkolnik, E.L., Southworth, J., Teske, J., Tremblin, P., Tucker, G.S., Venot, O., Waalkes, W.C., Welbanks, L., Zhang, X., Zieba, S., 2023. Early release science of the exoplanet WASP-39b with JWST NIRSpec PRISM. Nature 614 (7949), 659–663. http://dx.doi.org/10.1038/s41586-022-05677-y.

Selsis, F., Kasting, J.F., Levrard, B., Paillet, J., Ribas, I., Delfosse, X., 2007. Habitable planets around the star gliese 581? Astron. Astrophys. 476 (3), 1373–1387.

Shulyak, D., Lara, L.M., Rengel, M., Nèmec, N.E., 2020. Stellar impact on disequilibrium chemistry and observed spectra of hot jupiter atmospheres. Astron. Astrophys. 639, A48. http://dx.doi.org/10.1051/0004-6361/201937210, arXiv:2005.01470.

Stock, J.W., Kitzmann, D., Patzer, A.B.C., Sedlmayr, E., 2018. FastChem: A computer program for efficient complex chemical equilibrium calculations in the neutral/ionized gas phase with applications to stellar and planetary atmospheres. Mon. Not. R. Astron. Soc. 479 (1), 865–874.

Teal, D.J., Kempton, E.M.-R., Bastelberger, S., Youngblood, A., Arney, G., 2022. Effects of UV stellar spectral uncertainty on the chemistry of terrestrial atmospheres. Astrophys. J. 927 (1), 90. http://dx.doi.org/10.3847/1538-4357/ac4d99, arXiv:2201.08805.

Tsai, S.-M., Lee, E.K.H., Powell, D., Gao, P., Zhang, X., Moses, J., Hébrard, E., Venot, O., Parmentier, V., Jordan, S., Hu, R., Alam, M.K., Alderson, L., Batalha, N.M., Bean, J.L., Benneke, B., Bierson, C.J., Brady, R.P., Carone, L., Carter, A.L., Chubb, K.L., Inglis, J., Leconte, J., Line, M., López-Morales, M., Miguel, Y., Molaverdikhani, K., Rustamkulov, Z., Sing, D.K., Stevenson, K.B., Wakeford, H.R., Yang, J., Aggarwal, K., Baeyens, R., Barat, S., de Val-Borro, M., Daylan, T., Fortney, J.J., France, K., Goyal, J.M., Grant, D., Kirk, J., Kreidberg, L., Louca, A., Moran, S.E., Mukherjee, S., Nasedkin, E., Ohno, K., Rackham, B.V., Redfield, S., Taylor, J., Tremblin, P., Visscher, C., Wallack, N.L., Welbanks, L., Youngblood, A., Ahrer, E.-M., Batalha, N.E., Behr, P., Berta-Thompson, Z.K., Blecic, J., Casewell, S.L., Crossfield, I.J.M., Crouzet, N., Cubillos, P.E., Decin, L., Désert, J.-M., Feinstein, A.D., Gibson, N.P., Harrington, J., Heng, K., Henning, T., Kempton, E.M.-R., Krick, J., Lagage, P.-O., Lendl, M., Lothringer, J.D., Mansfield, M., Mayne, N.J., Mikal-Evans, T., Palle, E., Schlawin, E., Shorttle, O., Wheatley, P.J., Yurchenko, S.N., 2023. Photochemically produced SO_2 in the atmosphere of WASP-39b. Nature 617 (7961), 483–487. http://dx.doi.org/10.1038/s41586-023-05902-2, arXiv:2211.10490.

Tsai, S.-M., Lyons, J.R., Grosheintz, L., Rimmer, P.B., Kitzmann, D., Heng, K., 2017. VULCAN: An open-source, validated chemical kinetics python code for exoplanetary atmospheres. Astrophys. J. Suppl. Ser. 228 (2), 20. http://dx.doi.org/10.3847/1538-4365/228/2/20.

Tsai, S.-M., Malik, M., Kitzmann, D., Lyons, J.R., Fateev, A., Lee, E., Heng, K., 2021. A comparative study of atmospheric chemistry with VULCAN. Astrophys. J. 923 (2), 264. http://dx.doi.org/10.3847/1538-4357/ac29bc.

Venot, O., Hébrard, E., Agúndez, M., Dobrijevic, M., Selsis, F., Hersant, F., Iro, N., Bounaceur, R., 2012. A chemical model for the atmosphere of hot jupiters. Astron. Astrophys. 546, A43. http://dx.doi.org/10.1051/0004-6361/201219310.

Zahnle, K., Marley, M.S., Fortney, J.J., 2009. Thermometric soots on warm jupiters? arXiv e-prints arXiv:0911.0728.

Zamyatina, M., Hébrard, E., Drummond, B., Mayne, N.J., Manners, J., Christie, D.A., Tremblin, P., Sing, D.K., Kohary, K., 2023. Observability of signatures of transport-induced chemistry in clear atmospheres of hot gas giant exoplanets. Mon. Not. R. Astron. Soc. 519 (2), 3129–3153. http://dx.doi.org/10.1093/mnras/stac3432.